Nanoscale

Accepted Manuscript

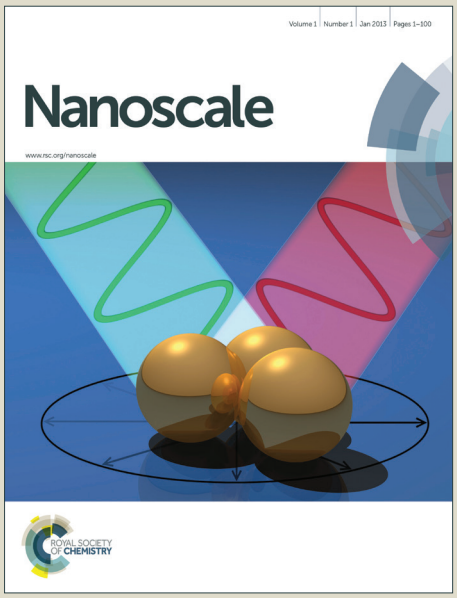

This is an *Accepted Manuscript*, which has been through the Royal Society of Chemistry peer review process and has been accepted for publication.

Accepted Manuscripts are published online shortly after acceptance, before technical editing, formatting and proof reading. Using this free service, authors can make their results available to the community, in citable form, before we publish the edited article. We will replace this *Accepted Manuscript* with the edited and formatted *Advance Article* as soon as it is available.

You can find more information about *Accepted Manuscripts* in the Information for Authors.

Please note that technical editing may introduce minor changes to the text and/or graphics, which may alter content. The journal's standard Terms & Conditions and the Ethical guidelines still apply. In no event shall the Royal Society of Chemistry be held responsible for any errors or omissions in this *Accepted Manuscript* or any consequences arising from the use of any information it contains.

ROYAL SOCIETY OF CHEMISTRY

www.rsc.org/nanoscale

Please do not adjust margins

Journal Name

ARTICLE

Understanding the growth and composition evolution of gold-seeded ternary InGaAs nanowires

A. S. Ameruddin*[a,b], P. Caroff [a], H.H. Tan [a], C. Jagadish [a] and V. G. Dubrovskii*[c-e]

Received 00th June 2015,
Accepted 00th xxxx 20xx,

DOI: 10.1039/x0xx00000x

www.rsc.org/

InGaAs nanowires offer great promise in fundamental studies of ternary compound semiconductors with variable composition and opens up wide a range of applications due to their bandgap tunability and high carrier mobility. Here, we report a study on growth of Au-seeded InGaAs nanowires by metal-organic vapour phase epitaxy and present a model to explain the mechanisms that govern the growth and composition evolution in ternary III-V nanowires. The model allows us to further understand the limitations on the growth rate and incorporation of the two group III species imposed by the deposition conditions and some intrinsic properties of the material transport and nucleation. Within the model, the evolution of InGaAs nanowire growth rate and composition with particle size, temperature and V/III ratio are described and correlate very well with experimental findings. The understanding gained in this study should be useful for the controlled fabrication of tunable ternary nanowires for various applications.

1. Introduction

Metal-seeded vapour-liquid-solid (VLS) III-V nanowires have proven their advantages for various applications in optoelectronics [1], nanoelectronics [2] and quantum transport physics [3]. Within the vast majority of nanowire structures, ternary nanowires are less studied as compared to the binary systems. Ternary nanowires are interesting as they allow for the desired bandgap tunability simply by changing the alloy fraction of the ternary compound, which is almost insensitive to material segregation and lattice mismatch issues in VLS systems. However, they bring additional complexity in terms of understanding and control because of compositional and structural inhomogeneity due to segregation, intermixing, different diffusion coefficients for each species, composition-dependent crystal structure [4-5], and differing incorporation pathways for each element at the Au droplet-nanowire interface or on the exposed sidewalls [6-9]. Improving our fundamental understanding of ternary nanowire growth and composition evolution as a function of directly accessible experimental parameters would therefore be crucial to achieve better control over the device structures. Among the wide range of III-V ternary compounds, the InGaAs system is one of the most interesting because of several key properties such as its tunable direct bandgap between 0.350 and 1.424 eV and the possibility of perfect lattice matching with InP ($In_{0.53}Ga_{0.47}As$), making it an ideal system for optical telecommunications. InGaAs material also has a very high carrier mobility (μ_e=~10000 $cm^2V^{-1}s^{-1}$, μ_h=~300 $cm^2V^{-1}s^{-1}$), which is highly interesting for monolithic integration with state-of-the-art complementary metal oxide semiconductor (CMOS) technology [10-11].

Despite recent interest [12-13], true understanding and modeling of ternary III-V nanowires obtained by the VLS mechanism with Au catalysts is still lacking. This is due to several issues such as: (i) complex equilibrium phase diagrams and non-equilibrium chemical potentials of quaternary alloys such as Au-Ga-In-As in our case [14], (ii) uncertainties in determining the composition of the initial critical nucleus even if both Au droplet and solid compositions were exactly known, (iii) absence of any data on relevant surface energies of different interfaces and (iv) lack of reliable data on the kinetic parameters (diffusion lengths, desorption rates of As etc.) as functions of the composition. Therefore, the existing approach based on chemical potentials, surface energies, and the

[a]Department of Electronic Materials Engineering, Research School of Physics and Engineering, The Australian National University, Canberra ACT 2601, Australia.
*Email: amira.ameruddin@anu.edu.au
[b]Faculty of Science, Technology and Human Development, Universiti Tun Hussein Onn Malaysia, PArit Raja 86400, Johor, Malaysia
[c]St. Petersburg Academic University, Khlopina 8/3, 194021, St. Petersburg, Russia
[d]Ioffe Physical Technical Institute RAS, Politekhnicheskaya 26, 194021, St. Petersburg, Russia
[e]ITMO University, Kronverkskiy pr. 49, 197101 St.Petersburg, Russia
*Email: dubrovskii@mail.ioffe.ru

Nanoscale Accepted Manuscript

Please do not adjust margins

Zeldovich nucleation rate for macroscopic islands [15-17] may require some crude assumptions which cannot be easily checked against experimental data. Consequently, here we systematically study the growth of InGaAs nanowires under different conditions and develop a simple model for complex growth phenomena in InGaAs nanowires which is capable of describing the main experimental trends and might serve as the first step toward establishing a more advanced understanding.

2. Experimental details

InGaAs nanowires were grown using metal-organic vapour phase epitaxy (MOVPE) with Trimethylgallium (TMGa), Trimethylindium (TMIn) and Arsine (AsH_3) as metal and arsenic precursors, respectively. GaAs (111)B substrates were treated with poly-L-lysine and Au colloid solution with diameter ranging from 10 nm to 80 nm for seeding the nanowire growth. Prior to growth, the substrates were annealed at 600 °C for 10 minutes to enable nucleation of the alloy particles. The nanowire growth temperature was varied between 400 and 525 °C. V/III ratio was also varied, ranging from 1.4 to 86.0. The mole fraction of TMIn/(TMIn+TMGa) was fixed at 0.30 throughout all the experiments.

Nanowires were then characterized using a ZEISS UltraPlus field-emission scanning electron microscope (FE-SEM) and a JEOL 2100F scanning transmission electron microscope (STEM). The lengths of the nanowires were measured on more than 20 nanowires per sample. Energy-dispersive x-ray (EDX) measurements for the solid composition of the nanowires were performed in STEM mode for at least 3 nanowires per sample along the [110] or [1120] zone axis of ~100 nm areas beneath the seed nanoparticle.

3. Results and discussion

3.1 Experimental results

The Au-seeded growth of InGaAs nanowires in MOVPE reactor is illustrated in Fig. 1. The TMIn, TMGa and AsH_3 precursors arrive at different surfaces from vapour in a given proportion, dissociate at a certain temperature-dependent rates, and incorporate to the sidewalls by the vapour-solid (VS) or onto the nanowire tops by the VLS mechanisms. The two competing mechanisms that govern the growth determine the final morphology of the nanowire. The Au droplet size, however, should be preserved during steady-state growth.

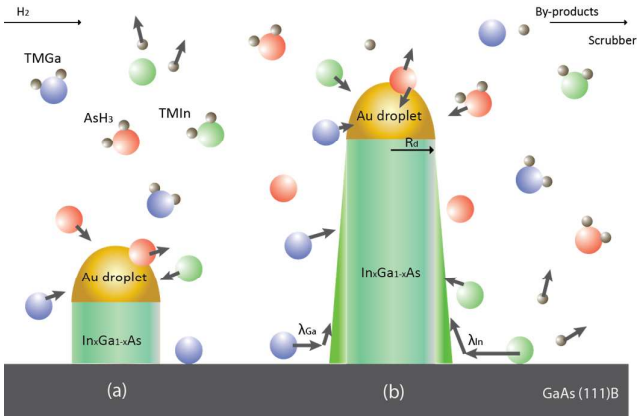

Fig. 1. Schematics of Au-assisted InGaAs nanowire growth in MOVPE reactor. The VLS growth in (a) results in a time-independent radius while the combination of VLS and VS growths in (b) yields nanowires with tapered morphology. The TMGa, TMIn and AsH_3 precursors decompose into Ga, In and As, respectively, releasing by-products. The As atoms incorporate only via the VLS mode while Ga and In adatoms are able to diffuse to the Au droplet from the nanowire sidewalls, with the diffusion lengths λ_{Ga} and λ_{In}, respectively.

Here we present several series of samples in which the final nanowire axial growth rates and compositions are determined as functions of different experimentally controlled conditions. The parameters that are expected to influence the nanowire growth and composition are: Au droplet diameter, V/III flow ratio in vapour and growth temperature. For the Au droplet diameter dependent experiments, the growth was carried out with a fixed growth temperature of 500 °C and V/III ratio of 2.4. The morphology of differently sized nanowires is shown in the SEM images in Fig. 2.

In general, these InGaAs nanowires exhibit a non-monotonic dependence of the axial growth rate and morphology on the Au droplet diameter. Nanowires seeded with particles up to 30 nm are shorter and have uniform diameter from base to top apart from the relatively large pyramidal base. These nanowires also have smooth sidewalls. As the diameter increase to 50 nm, the nanowires get much longer and show a smaller degree of tapering. The 80 nm seeded nanowires are shorter than the 50 nm ones and show a larger degree of tapering. Faceting and the rough sidewalls are also noticeable on the larger diameter nanowires. This normally indicates the crystal phase transitions in such nanowires [18]. The In percentage χ_{In} (%) in the InGaAs alloy in nanowires seeded with differently sized Au droplets was extracted and plotted along with the average axial growth rate dL/dt (nm/min) versus the Au droplet diameter in Fig. 3. Note that χ_{In} is extracted from EDX measurement of few nanowires taken from each samples with the electron beam focused on the top area of the nanowire as shown in Fig. 2 (f). Careful consideration is taken to ensure that the electron beam is not in the area right below the Au droplet where axial growth could have occurred during cooling down.

Nanoscale Accepted Manuscript

This journal is © The Royal Society of Chemistry 20xx

Please do not adjust margins

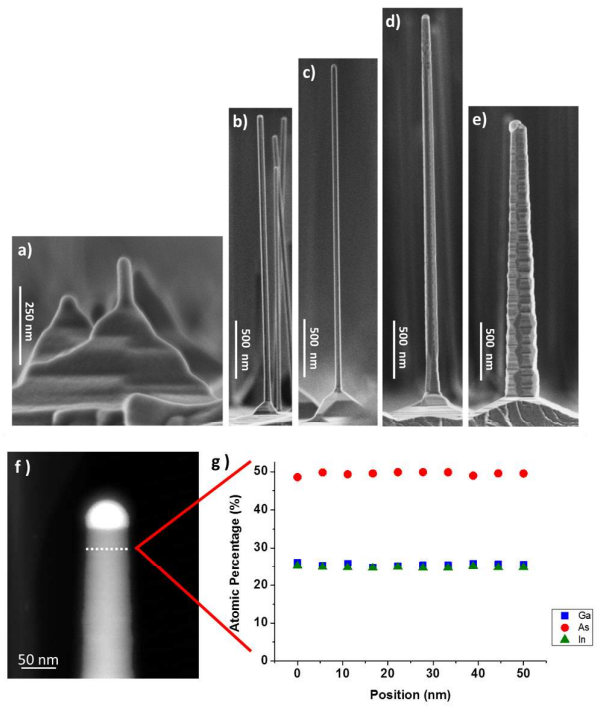

Fig 2. The SEM cross-section views of InGaAs nanowires seeded by a) 10 nm b) 20 nm c) 30 nm d) 50 nm and e) 80 nm diameter Au nanoparticles. f) High-annular angular dark field (HAADF) STEM image of a nanowire grown with 50 nm Au droplet. The dotted line represents the region where EDX measurements are taken. g) The corresponding composition as measured by the EDX in (f).

Details on the experimental studies of other parameters influencing the nanowire morphology and dimensions can be found in our previous work [19]. Here, we closely investigate the axial growth rate and the In percentage in solid as functions of the V/III ratio and the growth temperature, for which the experimental data are shown in Figs. 4 and 5, respectively. Since the experimentally observed behaviours are complex and non-linear, below we present a model to rationalize these findings.

3.2 Model Approach

First and most importantly, we assume that the relative atomic concentrations of In and Ga are the same in the liquid and solid state, i.e. the nanowire composition is given by

$$\chi_{In} = \frac{C_{In}}{C_{In}+C_{Ga}}; \quad \chi_{Ga} = \frac{C_{Ga}}{C_{In}+C_{Ga}}, \tag{1}$$

where C_{In} and C_{Ga} are the atomic concentrations of In and Ga atoms in the Au droplet. This implies a transport-limited regime of nanowire growth rather than a nucleation-limited growth mode in which the liquid and solid composition can be very different for many reasons (preferential nucleation and/or two-dimensional growth of one compound versus the other, non-stoichiometric nuclei etc.) [8,20,21]. While the nucleation-limited regime should be described by the Zeldovich nucleation rate [17], some recent studies revealed that we really approach the limit of macroscopic theory in such modeling even for binaries. For instance, the critical size of Au-catalyzed GaAs nanowires grown by hydride vapour phase epitaxy approaches 1 III-V pair [17] and equals only 2 III-V pairs in Ga-catalyzed GaAs nanowires [22]. Clearly, the classical model for macroscopic island with well-defined boundaries is hardly suited to describe such situations.

In order to eliminate most of these uncertainties and in line with the first assumption on the uniform composition, we write the nucleation rate, J in the form of $J = \sigma D_{As} n_{As}^L (n_{In}^L + n_{Ga}^L)$, as in the irreversible growth models [23,24]. Here, D_{As} is the As diffusion coefficient in liquid, n_k^L are the surface concentration of atoms of species $k(k = As, In, Ga)$ at the liquid-solid interface and σ is the capture rate which is assumed identical for $k = In, Ga$. Otherwise, the nanowire composition would differ from the liquid one due to different aggregation probabilities of InAs and GaAs. Assuming also a spatially homogeneous composition in the Au droplet due to its small dimension and high diffusivities in liquid at the typical growth temperatures, we can write $n_k^L = (h/\Omega)c_k$, with h as the height of a monolayer and Ω as the volume per III-V pair in the solid state. More details regarding the transformation from macroscopic nucleation to regular irreversible growth in Au-catalyzed III-V nanowires are given in Ref. [23]. Using the atomistic growth picture, we can thus write the second central assumption of our model in the form of

$$J = \sigma D_{As} \left(\frac{h}{\Omega}\right)^2 c_{As}(c_{In} + c_{Ga}). \tag{2}$$

This nucleation rate gives the probability of nucleation per unit surface area. Hence the nanowire elongation rate can be approximated as

$$\frac{dL}{dt} = h\pi R_d^2 J, \tag{3}$$

where R_d is the radius of the nanowire top. Here, we assume that the nucleation is effectively mononuclear [15] although the critical size is close to one. This holds only for narrow facets but in fact Eq. (3) will affect the resulting growth rate only for small enough R.

For the diffusion transport of both group III species, we adopt the following simple expressions [15]:

$$j_k = 2V_k \left[1 + \frac{\lambda_k}{R_d}\left(1 - \frac{c_k}{c_k^A}\right)\right] \tag{4}$$

for $k = In, Ga$, written for hemispherical Au droplet with the radius equivalent to the radius of the nanowire top, R_d. Here V_k are the atomic vapour influx of group III species, both accounting for the temperature-dependent cracking efficiencies of TMIn and TMGa [25]. The $\lambda_k = \sqrt{D_k \tau_k}$ are the effective diffusion lengths of the group III adatoms on the sidewalls (influenced by the As flux), D_k are the diffusion coefficients of In and Ga adatoms, τ_k are their effective lifetimes (limited by radial growth) and $c_k^A = V_k \tau_k / h$ are the effective adatom activities on the sidewalls. The first terms in Eq. (4) describe the direct vapour flux and the second represent the surface diffusion of In and Ga adatoms [15,26-

Nanoscale Accepted Manuscript

Please do not adjust margins

29]. Desorption of both group III species from the Au droplet is insignificant and hence neglected at the typical growth temperatures between 400 and 525 °C [30, 15].

In the first approximation, the radial growth rate on the nanowire sidewalls is independent of height, and hence the nanowire shape is conical for the combined VLS-VS and cylindrical for the purely VLS incorporation pathways, as shown in Fig. 1. This radial growth can be well described within our model but is not elaborated here, since it does not affect the composition of VLS-grown nanowire cores, constituting the major fraction of the nanowire material.

The Au droplet can maintain a time-independent radius R_d, only when the material influxes of group III atoms into the Au droplet equal their sink due to nanowire growth, i.e.

$$\chi_k \frac{dL}{dt} = j_k \qquad (5)$$

for $k = In, Ga$. Summing up two Eqs. (5) for In and Ga, we obtain: $dL/dt = j_{In} + j_{Ga}$, which gives the transport-limited elongation rate. Neglecting surface diffusion of As species [24,31,32] and accounting for its desorption from the Au droplet, the As-limited elongation rate in the steady state is given by [33]:

$$\frac{dL}{dt} = 2\left[V_{As}(1+\varepsilon) - \nu_{As}^{des}\exp(R_{GT}/R_d)c_{As}\right], \qquad (6)$$

where V_{As} is the direct atomic flux of As and ε describes possible re-emission of As species. Desorption of As atoms from the Au droplet is assumed as being proportional to the As concentration with a certain temperature-dependent coefficient ν_{As}^{des}. Additionally, we take into account the Gibbs-Thomson (GT) effect [26-28] which exponentially increases As desorption from small Au droplets due to curvature effect, with a certain characteristic GT radius R_{GT}.

Solution to the above system can be obtained in simple analytical form if $D_{Ga}/\lambda_{Ga} \cong D_{In}/\lambda_{In}$ meaning that the reverse diffusion fluxes from the Au droplet onto the nanowire sidewalls is the same for both group III species. In this case, the composition is not influenced by the reverse diffusion fluxes from the Au droplet [the $-c_k/c_k^A$ terms in Eq. (4)] and equals

$$\frac{c_{Ga}}{c_{In}} = \frac{V_{Ga}}{V_{In}}\frac{(R_d+\lambda_{Ga})}{(R_d+\lambda_{In})}. \qquad (7)$$

The solid composition could diverge from Eq. (7) due to (i) different dimerization rates of InAs and GaAs pairs [neglected earlier in Eq. (2)] and (ii) different sinks of In and Ga atoms in the Au droplet, lumped together in the parameters $D_k/\lambda_k\,\sigma_k$ for k = Ga and In. A more detailed analysis of the model, which is beyond the scope of this paper, can be developed to cover the case for the parameters outside the study presented here.

The nanowire axial growth rate is obtained in the form of

$$\frac{dL}{dt} = \frac{y}{(2A+y)}2\widetilde{V}_{As}; y = \sqrt{(1+A-B)^2+4AB} - (1+A-B). \qquad (8)$$

The coefficients are given by

$$A = \left(\frac{R_0}{R_d}\right)^3 \exp\left(\frac{R_{GT}}{R}\right); R_0^3 \equiv \frac{2\nu_{As}^{des}}{\widetilde{V}_{As}}\frac{D_{In}}{\pi\lambda_{In}D_{As}\sigma}\left(\frac{\Omega}{h}\right)^2; B = \frac{\widetilde{V}_{In}+\widetilde{V}_{Ga}}{\widetilde{V}_{As}}, \qquad (9)$$

where $\widetilde{V}_{As} = V_{As}(1+\varepsilon)$; $\widetilde{V}_{In} = V_{In}(1+\lambda_{In}/R_d)$and $\widetilde{V}_{Ga} = V_{Ga}(1+\lambda_{Ga}/R_d)$are the total influxes of As, In and Ga atoms into the Au droplet, respectively.

3.3 Adequation between the model and experimental results

Firstly, we note that the composition of the ternary solid generally differs from the vapour composition. This effect has been previously reported in Refs. [34-37]. From Eq. (7), the nanowire composition in our model can be different from the vapour composition for two reasons: (i) different diffusion lengths of In and Ga adatoms and (ii) different cracking efficiencies of TMIn and TMGa at the growth temperature. We remind that V_{Ga}/V_{In} gives the ratio of the group III influx entering the Au droplet but not of the precursor fluxes impinging the Au droplet. Higher In composition in the nanowires than in vapour requires either $\lambda_{Ga} < \lambda_{In}$or $V_{Ga} < V_{In}$. The former inequality is well known since indium is a faster diffuser than gallium [15]. The latter inequality is supported, e.g., by the data of Ref. [25] showing that TMIn is a low-temperature precursor while the decomposition of TMGa at the solid surface starts only at above 400 °C and might be very sensitive to the group V flux. Hence the composition of the InGaAs alloy in solid will be affected by the growth conditions.

Figure 3 shows the graph of the composition of the InGaAs nanowire and the axial growth rate versus the Au droplet diameter at 500 °C, V/III ratio = 2.4 and Ga/In ratio = 7/3 in vapour. From Eq. (7), the In composition is expected to gradually decrease with the Au droplet size due to lower diffusion flux, and reach the vapour composition at $R \to \infty$. From Eqs. (8) and (9), the axial growth rate must first increase with R as R^2, then reaches a maximum and further decreases to a constant, as in most growth models for binary nanowires [15,27,29,31]. The solid lines in Fig. 3 show the fits that are obtained with appropriate parameters. In particular, the best fits are obtained with zero Ga diffusivity ($\lambda_{Ga} = 0$) even at the lowest V/III ratio of 2.4 so that the Ga diffusion should be ineffective in all cases. While certainly important for molecular beam epitaxy growth of GaAs nanowires, the fact that Ga diffusion can be disabled in the MOCVD case has previously been noticed by many authors (see chapter 5, Ref. [15] for a review). Hence, our data indicate that Ga incorporates mainly by direct impingement while In have additional incorporation via migrations of In to the Au droplet from the nanowire sidewalls. With $\lambda_{Ga} = 0$, the fits shown in Fig. 3 are obtained at $\lambda_{In} = 57$nm, $R_0 = 7$ nm and $R_{GT} = 9$ nm. We also assume that the cracking efficiencies for TMIn and TMGa equal one at 500 °C according to Stringfellow [25], in which case so that the ratio of Ga to In vapour atomic influxes, $V_{Ga}/V_{In} = 7/3$ is given by the vapour composition. No re-emission of As is required to obtain the fits ($\varepsilon = 0$) and thus $\widetilde{V}_{As} = V_{As}$, $V_{Ga} = 0.292 \times V_{As}$ and $V_{In} = 0.125 \times V_{As}$. We use the value of $V_{As} = 71$ nm/min for the overall normalization of the growth rates.

Nanoscale Accepted Manuscript

This journal is © The Royal Society of Chemistry 20xx

Please do not adjust margins

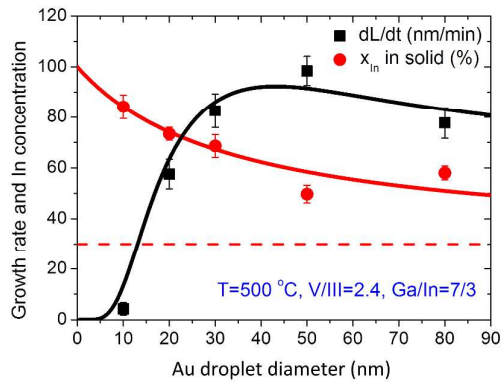

Fig. 3. Experimentally determined nanowire composition and axial growth rate versus Au droplet diameter at fixed *T*=500 °C, V/III ratio = 2.4 and nominal Ga/In = 7/3 in vapour (symbols), fitted by the model expressions (solid lines). The dotted lines represent x_{In} in vapour.

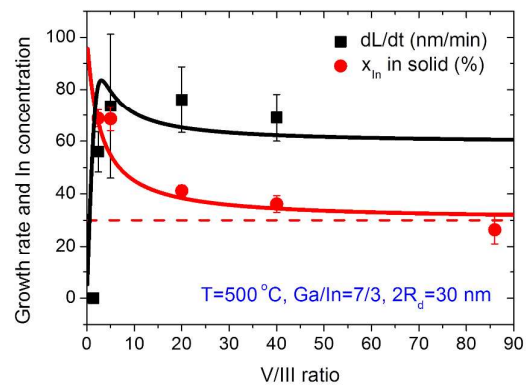

Fig 4. Experimentally determined nanowire composition and axial growth rate versus V/III ratio in vapour at fixed *T*=500 °C, nominal Ga/In = 7/3 in vapour and $2R_d$ =30 nm (symbols), fitted by the model expressions (lines). The dotted lines represent x_{In} in vapour.

Figure 4 depicts the behaviour of dL/dt and χ_{In} with V/III ratio at a fixed growth temperature of 500 °C and Ga/In ratio = 7/3, for 30 nm diameter seed particles. From Eq. (7), the In content decreases for higher V/III ratios due to a lower diffusivity of In adatoms [15], while the growth rate should feature a non-monotonic behaviour with III/V ratio. Eventually, raising the V/III ratio has the same effect on the dL/dt as increasing the Au droplet size. For low V/III ratios and small R_d, growth and composition are limited by As transport in the excess of group III atoms (where In should reach very high concentrations as a faster diffuser). As the Au droplet size or V/III ratio increases, the VLS growth is transformed to a group-III limited transport regime such that the growth rate decreases with R_d and V/III ratio and saturates to a constant. As mentioned earlier, the Ga diffusivity is put to zero for all V/III ratios ($\lambda_{Ga} = 0$). Hence only the suppression of the In diffusivity for higher V/III ratios is taken into account. For that purpose, we assume that the diffusion length of In scales with the As flux as $\lambda_{In} \propto 1/V_{As}$, i.e., the upward path of In adatoms decreases inversely proportional to the V/III flux ratio.

Finally, the temperature dependences of the dL/dt and χ_{In} should be non-monotonic. At low temperatures, the cracking efficiency of TMGa and the diffusion length of In adatoms tend to zero, which suppresses the axial growth rate, while at high temperatures the VLS growth is suppressed by the As desorption. The In content in solid should tend to unity at low temperatures due to a low cracking efficiency of TMGa. It should also reach a high value at elevated temperatures due to enhanced thermally activated diffusion of In adatoms. These trends correspond to our experimental data, as shown in Fig. 5.

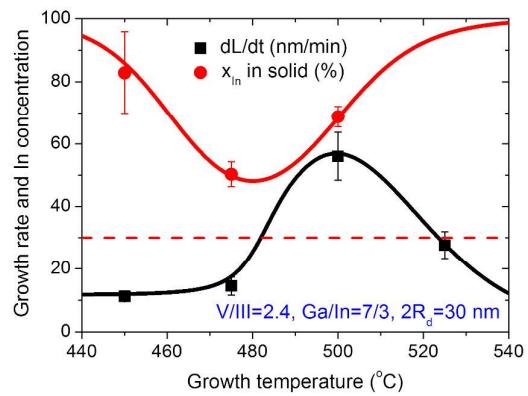

Fig. 5. Nanowire composition and axial growth rate versus growth temperature at fixed V/III ratio = 2.4, nominal Ga/In = 7/3 in vapour and $2R_d$ = 30 nm, (symbols), fitted by the model expressions (lines). The dotted lines represent x_{In} in vapour.

Fitting the temperature dependences of χ_{In} and dL/dt require some additional parameters. We use the Arrhenius temperature dependences of the In diffusion length and the coefficient A in Eq. (9) in the form $\lambda_{In} \propto \exp(-T_\lambda/T)$ and $A \propto \exp(-T_{des}/T)$ (assuming that the temperature dependence of A is dominated by the enhanced desorption of As through ν_{As}^{des}, with rather high values of the corresponding characteristic temperatures $T_\lambda = 6000\,K$ and $T_{des} = 15000\,K$. The observed decrease of the growth rate toward lower temperatures can be attributed only to the low cracking efficiencies of TMGa at low temperatures. For the latter, we use the temperature dependence of Ref. [34]: $V_{Ga} \propto (1/2)[1 + \tanh((T - T_{Ga})/\Delta T_{Ga})$ with the characteristic temperature of TMGa decomposition, T_{Ga} around 480°C and very narrow transition width, ΔT_{Ga} of the order of 10°C.

Thus, with a plausible set of parameters, the model is capable of describing all the observed experimental dependences, namely the growth rate and composition versus the Au droplet diameter, V/III flow ratio and temperature.

Nanoscale Accepted Manuscript

Please do not adjust margins

Conclusions

In summary, we have studied the growth and compositional evolution of InGaAs nanowires over a range of parameters. The composition and the axial growth rate are found to be highly dependent on the seed particle size and the deposition conditions. A simple model is established to explain the observed trends and in particular to quantify the differences between the nanowire and vapour compositions. It was found that the small diameter and low V/III ratio VLS growths proceed in the As-limited regime while the evolution of larger diameter nanowires at higher V/III ratios is governed by the group III transport. We observe that In content in nanowires is usually noticeably larger than that in vapour. This effect is explained by high In diffusivities at higher temperatures and low cracking efficiencies of TMGa at lower temperatures. InGaAs nanowire growth is most uniform when axial growth is maximized and radial growth is limited [19]. This condition is predicted to be in the As-limited regime by the model. However, the composition was far from the vapour composition. Nonetheless, we believe composition tunability can be achieved with high uniformity by simply tuning the In/Ga in vapour in this regime.

Further studies should include non-stationary growth effects such as nucleation pulses [37] and switching between the two group III precursors when forming the nanowire heterostructures, as well as possible inhomogeneity of the composition along the nanowires length or width. In particular, the In-rich shell can be observed due to the VS radial growth on the sidewalls where there are more In adatoms due to a better cracking efficiency and/or surface diffusion length of In with respect to Ga. Overall, the obtained results and theoretical understanding shed more light on the complex growth phenomena in Au-seeded ternary III-V nanowires and allow for a better control over the nanowire composition by tuning their size and the growth parameters.

Acknowledgements

This research was supported by The Australian Research Council. We acknowledge Australian National Fabrication Facility and Australian Microscopy and Microanalysis Research Facility for access to facilities used ion this work. V. G. D. gratefully acknowledges financial support of the Russian Foundation for Basic Research under grants 13-02-00622, 13-02-12045, 15-52-78057 and 15-52-53041. A. S. A. would like to acknowledge the Malaysian Ministry of Education for her scholarship.

References

1 X. Duan, Y. Huang, R. Agarwal and C. M. Lieber *Nature*, 2006 **421**, 241-245.
2 E. Lind, A. I. Persson, L. Samuelson and L. Wernersson, *Nano Lett.,* 2006, **6** (9), 1842–1846.
3 C. Thelander, M.T. Björk, M.W. Larsson, A.E. Hansen, L.R. Wallenberg and L. Samuelson, *Solid State Comm.* 2004, **131** (9-10), 573–579.
4 G. Koblmüller and G. Abstreiter, *Phys. Status Solidi RRL*, 2013, 1–20.
5 C.S. Jung, H.S. Kim, G.B. Jung, K.J. Gong, Y.J. Cho, S.Y. Jang, C.H. Kim, C. Lee and J. Park, *J. Phys. Chem*., 2011, **115**, 7843-7850.
6 C. Chen, S. Shehata, C. Fradin, R. LaPierre, C. Couteau, and G. Weihs, *Nano Lett.*, 2007, **7** (9), 2584-2589.
7 Y.Kim, H.J. Joyce, Q. Gao, H.H. Tan, C. Jagadish, M. Paladugu, J. Zou and A.A. Suvorova, *Nano Lett.* 2006, **6** (4), 599-604.
8 Y.-N. Guo, H.-Y. Xu, G.J. Auchterlonie, T. Burgess, H.J. Joyce, Q. Gao, H.H. Tan, C. Jagadish, H.-B. Shu, X.-S. Chen, W. Lu, Y. Kim, and J. Zou, *Nano Lett*., 2013, **13**, 643.
9 J. Wu, B.M. Borg, D, Jacobsson, K.A. Dick, L.-E. Wernersson, *J. Cryst. Growth*, 2013, **383**, 158-165.
10 T. Irisawa, M. Oda, K. Ikeda, Y. Moriyama, E. Mieda, W. Jevasuwan, T. Maeda, O. Ichikawa, T. Osada, M. Hata, Y. Miyamoto, T. Tezuka, *Electron Dev. Meeting 2013, IEEE Int.,* 2.2.1-2.2.4.
11 A. Thean, N. Collaert, I. P. Radu, N. Waldron, C. Merckling, L. Witters, R. Loo, J. Mitard, R. Rooyackers, A. Vandooren, A. Verhulst, A. Veloso, D. Yakimets, T. H. Bao, D. Chiappe, A. Vaysset, O. Zografos, M. Caymax, C Huyghebaert, K. Barla, and A. Steegen, *ECS Trans*., 2015, **66** (4), 3-14.
12 S.G. Ghalamestani, M. Ek, M. Ghasemi, P. Caroff, J. Johansson, and K.A. Dick, *Nanoscale*, 2014, **6**, 1086.
13 A. Fakhr and Y. M. Haddara, *J. Appl. Phys.*, 2014, **116**, 024314.
14 M. Ghasemi, B. Sundman, S.G. Fries, and J. Johansson, *J. Alloys and Compounds*, 2014, **600,** 178–185.
15 V.G. Dubrovskii, *Nucleation theory and growth of nanostructures*. Springer, Heidelberg – New York – Dordrecht – London, 2014.
16 F. Glas, *J. Appl. Phys.,* 2010, **108**, 073506.
17 V.G. Dubrovskii and J. Grecenkov, *Cryst. Growth Des.*, 2015, **15**, 340.
18 J. Bollinsson, P. Caroff, B. Mandl and K.A. Dick, *Nanotechnology*, 2011, **22**, 265606
19 A.S. Ameruddin, H.A. Fonseka, P. Caroff, J.W. -Leung, R.L.M.O. Veld, J.L. Boland, M.B. Johnston, H.H. Tan and C. Jagadish, *Nanotechnology*, 2015, **26**, 205604.
20 K.A. Dick, K. Deppert, L. Samuelson,L. R. Wallenberg, and F.M. Ross, *Nano Lett*., 2008, **8**, 4087.
21 J. Johansson, L. S. Karlsson, K. A. Dick, J. Bolinsson, B. A. Wacaser, K. Deppert, and L. Samuelson, *Cryst. Growth Des.*, 2009, **9**, 766.
22 F. Glas, M.R. Ramdani, G. Patriarche, and J.C. Harmand, *Phys. Rev. B*, 2013, **88**, 195304.
23 V.G. Dubrovskii, *J. Chem. Phys.,* 2015, **142**, 204702.
24 V.G. Dubrovskii and N.V. Sibirev, *Phys. Rev. B,* 2014, **89**, 054305.
25 G.B. Stringfellow, *Mat. Sci. Engineering B,* 2001, **87**, 97.
26 V.G. Dubrovskii, N.V. Sibirev, G.E. Cirlin, I.P. Soshnikov, W.H. Chen, R. Larde, E. Cadel, P. Pareige, T. Xu, B. Grandidier , J.-P. Nys, D. Stievenard, M. Moewe, L.C. Chuang, and C. Chang-Hasnain, *Phys. Rev. B*, 2009, **79**, 205316.
27 A. Fakhr, Y.M. Haddara, and R. R. LaPierre, *Nanotechnology,* 2010, **21**, 165601.
28 V.G. Dubrovskii, N.V. Sibirev, G.E. Cirlin, A. D. Bouravleuv, Yu.B. Samsonenko, D.L. Dheeraj, H.L. Zhou, C. Sartel, J.C. Harmand, G. Patriarche, and F. Glas, *Phys. Rev. B,* 2009, **80**, 205305.
29 V.G. Dubrovskii and Yu.Yu. Hervieu, *J. Cryst. Growth,* 2014, **401**, 431.
30 K. Muraki, S. Fukatsu, Y. Shiraki, and R. Ito, *Appl. Phys. Lett.*, 1992, **61** (5), 557.
31 M.R. Ramdani, J.C. Harmand, F. Glas, G. Patriarche, and L. Travers, *Cryst. Growth Des.*, 2013, **13**, 91.
32 G. Priante, S. Ambrosini, V.G. Dubrovskii, A. Franciosi, and S. Rubini, *Cryst. Growth Des.,* 2013 **13**, 3976.

Nanoscale Accepted Manuscript

This journal is © The Royal Society of Chemistry 20xx

Please do not adjust margins

33 A. Kelrich, V.G. Dubrovskii, Y. Calahorra, S. Cohen, and D. Ritter, *Nanotechnology*, 2015, **26**, 085303.
34 A.D. Bouravleuv, N.V. Sibirev, G. Statkute, G.E. Cirlin, H. Lipsanen, and V.G. Dubrovskii, *J. Cryst. Growth*, 2010, **312**, 1676
35 V. Dubrovskii, *Phys. Rev. B.*, 2013, **87**, 195426.

Nanoscale Accepted Manuscript

Please do not adjust margins